USA) in PBS(−). The blocking step was carried out using 5% calf serum in PBS(−) to avoid non-specific adsorption of the antibody and reduce the background signal. In fact, there was no significant non-specific binding of mouse IgG antibody against myotubes assessed by the enzyme-linked immunosorbent assay. The cells were immunostained using the mouse monoclonal anti-c-myc first antibody (Santa Cruz Biotechnology, Santa Cruz, CA, USA) overnight at 4 °C. Then, Alexa Fluor 594-conjugated anti-mouse IgG second antibody (Invitrogen Corp.) was bound to the first antibody for 1 h at room temperature. The immunostained gel sheet was mounted on a cover glass with Vectashield (Vector Laboratories, Burlingame, CA, USA). Fluorescent images were observed using a LSM 700 laser scanning microscope and the associated LSM software, ZEN 2009 (Carl Zeiss MicroImaging Co., Ltd, Tokyo, Japan).

Results and discussion

To achieve long-term minimally invasive stimulation of muscle cells, the electrodes were coated with PEDOT. Fig. 3 shows the micrographs of bare (A and B) and PEDOT-coated Pt microelectrodes (C and D). It is clear that the white shiny bare Pt microelectrode surface (A) was changed to black by the PEDOT modification (C). After the electrical pulse application (amplitude, 2 V; frequency, 1 Hz; duration, 10 ms) for 15 h in the EPS medium, the color of the bare Pt microelectrode changed to brown (B). This discoloration would be attributed to the electrochemical corrosion of the Pt layer, which means oxidation of the Pt layer at a high potential pulse cycle, followed by dissolution as the Pt ion into the medium.[21] On the other hand, the PEDOT-coated microelectrode showed no apparent morphological change even after 15 h of pulse application (Fig. 3(D)), and remained intact for more than 3 days pulse application. The PEDOT film of the electrode (D) was removed by aqueous sodium hypochlorite which causes over-oxidation and degradation of the PEDOT film,[22] which revealed that the underlying Pt microelectrodes remained intact (Fig. 3(E)). In addition to corrosion of the Pt layer, the faradaic reactions at the Pt electrode/medium interface cause drastic changes in culture conditions such as pH, which would injure the cells. In fact, we observed gas evolution, which was associated with water electrolysis at the bare Pt electrode, resulted in damaging the cells on the electrodes.[18] When using the PEDOT-coated microelectrode with a large surface electric capacity, the non-faradaic charging current will suppress unfavorable faradaic reactions and ensure stable long-term electric stimulation.

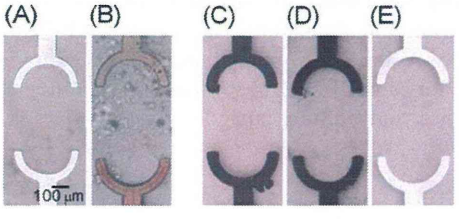

Fig. 3 Micrographs of bare (A and B) and PEDOT-coated Pt microelectrodes (C and D) before (A and C) and after (B and D) electrical pulse application (amplitude, 2 V; frequency, 1 Hz; duration, 10 ms) for 15 h in the EPS medium. (E) Pt microelectrode after detachment of PEDOT layer from the electrode D.

The electric field distribution on the microelectrode array was simulated by the finite element method using FEMLAB software (COMSOL 3.1, COMSOL AB, Sweden). The three-dimensional model geometry, including microelectrode arrays, mimicked those of the experimental setup. The simulated model microelectrode arrays did not include the electrode material properties. Fig. 4(A) shows a micrograph of the PEDOT microelectrode arrays and Fig. 4(B) shows the simulated electric field distribution for a model microelectrode array when a voltage of 2 V was applied between the central microelectrode pair. The electric field was concentrated between the active electrodes and did not spread out to the neighbouring regions. Fig. 4(C) shows the electric field distribution along the cross-section a–b in Fig. 4(B). The vertical axis in Fig. 4(C) represents the distance from the microelectrode surface. The simulated electric field rapidly decreased with increasing distance from the microelectrode surface. These data suggested that the electric field generated by the microelectrodes was effective only in the region near the microelectrode surface. Assuming the vertical axis in Fig. 4(C) to be the thickness of the gel, for effective electrical stimulation the myotubes/fibrin gel should be attached to the microelectrode array chip so that the side of the gel sheet with the transferred myotubes was in contact with the electrode surface.

Fig. 5(A) shows a phase-contrast micrograph of WT-C_2C_{12} myotube line patterns on the fibrin gel aligned with the PEDOT microelectrode arrays. During the alignment, the lined structure of the myotubes was maintained without detachment from the gel, allowing arbitrary and repetitive changes of the localized electrical stimulation site on the myotube line patterns. As can be seen in Fig. 5(A), the focus on the cells was matched with that of on the microelectrodes, suggesting the cells are in close vicinity of the electrode surface. The distance between the cells and the PEDOT layer was less than 100 μm, as assessed from the defocusing Z distance using a confocal microscopy. Fig. 5(B) shows the time courses of contractile displacements of myotube line patterns on the PEDOT microelectrode arrays when stimulated with periodic electrical pulses (amplitude, 2 V; frequency, 1 Hz; duration, 10 ms). Contractile displacement was determined from the real-time movie of myotube contraction shown in Movie S1, ESI†.

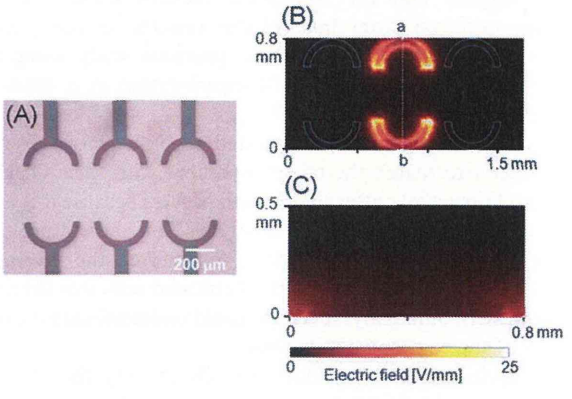

Fig. 4 (A) Micrograph of the PEDOT-coated microelectrode arrays. (B) Simulated electric field distribution for a model microelectrode array where a voltage of 2 V was applied between the central microelectrode pair. (C) Simulated electric field distribution along the cross-section a–b in (B).

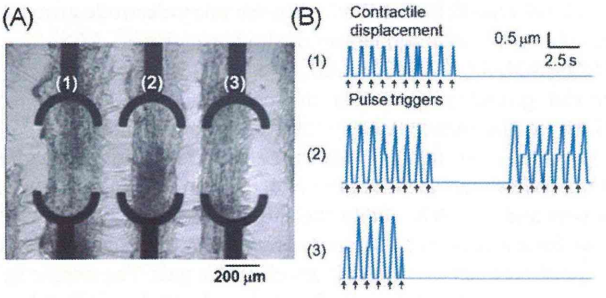

Fig. 5 (A) Phase-contrast micrograph of WT-C_2C_{12} myotube line patterns aligned with the microelectrode arrays. (B) Time course of myotube line patterns contraction stimulated with periodic electrical pulses (amplitude, 2 V; frequency, 1 Hz; duration, 10 ms). The arrows below the time course represent the pulse triggers.

Pulse triggers are indicated as arrows below each time course. The numbers (1) to (3) in Fig. 5(B) represent the contractile behavior of myotube line patterns labeled (1) to (3) in Fig. 5(A). At first, all the myotube line patterns were stimulated, followed by resting patterns (3) to (1) in order, and finally we selectively stimulated just pattern (2). Each myotube line pattern exhibited independent contractile behaviour synchronized with the electric pulse supplied through the aligned microelectrodes. These results suggested that contractile activity of each myotube line pattern could be arbitrarily controlled using the microelectrode arrays.

Fig. 6 depicts the expression assay of GLUT4 by the selective stimulation of the transfected myotube line patterns. Myotube line pattern on the left side was stimulated for 3.5 h at 10 Hz (amplitude, 2 V; duration, 3 ms; train, 1 s; interval, 10 s) and the right side pattern was rested, as shown in Movie S2, ESI†. The myotubes were immunostained with the anti-c-myc first antibody and the Alexa Fluor 594-conjugated anti-mouse IgG second antibody after the electrical stimulation and cell fixation. The antibodies used are impermeable to the cell membrane, which makes it enable to stain only the GLUT4 expressed on the cell surface.[19] As can be seen in Fig. 6(B) and (C), electrically stimulated myotubes displayed an obvious increase in fluorescent intensity above that of unstimulated cells by about 4-fold. This result suggests that the contraction-induced GLUT4 translocation occurred from intracellular vesicles to the plasma membrane, in agreement with our previous study using the western blot analysis of GLUT4 translocation in a random-cultured myotube monolayer.[19,20]

In a conventional random-cultured myotube monolayer, it was difficult to match the target myotubes with their GLUT4 translocation activity after the fixation process because it is hard to seek the "contracted target myotubes" on the culture dish during the electrical stimulation. Therefore, the averaged GLUT4 translocation activity of all cultured cells was detected by the western blot analysis, which would underestimate the true activity of the contractile myotubes.

Our device made it possible to easily identify the GLUT4 translocation activity of the contracting myotubes for the first time, by artificially patterning and locally targeted stimulation of the myotubes on the gel sheet. Furthermore, by patterning myotube lines subjected to different stimulation conditions next to each other, high-contrast imaging of the contraction effect on

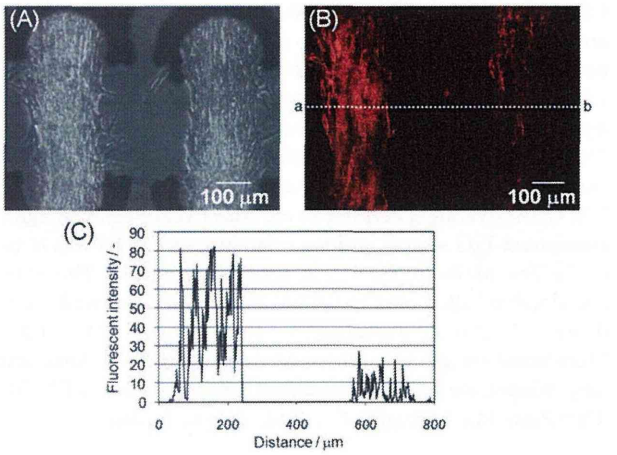

Fig. 6 (A) Phase-contrast micrograph of the transfected myotube line patterns locally stimulated with the PEDOT microelectrode arrays (amplitude, 2 V; duration, 3 ms; frequency, 10 Hz; train, 1 s; interval, 10 s). (B) Fluorescent image of the myotube line patterns immunostained with anti-c-myc first antibody and Alexa Fluor 594-conjugated anti-mouse IgG second antibody. (C) Fluorescent intensity of each immunostained myotube line pattern along the cross-section a–b in (B).

GLUT4 translocation in myotubes was achieved. This device would be applicable for quantitative bioassays of various contraction-induced metabolic alterations in myotubes.

Conclusions

We have developed a micropatterned C_2C_{12} myotubes/fibrin gel culture system integrated with a PEDOT microelectrode array chip for skeletal muscle cell-based bioassay. Arbitrary control of micropatterned myotubes contraction with localized electrical stimulation enabled high-contrast imaging of contraction-induced GLUT4 translocation phenomena in myotubes. This device would easily permit focusing the stimulation site on a desired specific tissue construct, such as a neuromuscular junction formed in a neuron–skeletal muscle cell co-culture. Such applications would be reported in future studies.

Acknowledgements

This work was supported by a Core Research for Evolutional Science and Technology grant from the Japan Science and Technology Agency, partly by Special Coordination Funds for Promoting Science and Technology, Formation of the Innovation Center for Fusion of Advanced Technologies from the Japan Science and Technology Agency, by the Research Grant Program of Asahi Glass Foundation, and by Grants-in-Aid for Scientific Research B (17310080) from the Ministry of Education, Science, and Culture, Japan.

References

1 J. El-Ali, P. K. Sorger and K. F. Jensen, Cells on chips, *Nature*, 2006, **442**, 403–411.
2 H. Aubin, J. W. Nichol, C. B. Hutson, H. Bae, A. L. Sieminski, D. M. Cropek, P. Akhyari and A. Khademhosseini, Directed 3D cell alignment and elongation in microengineered hydrogels, *Biomaterials*, 2010, **31**, 6941–6951.

3 J. T. Lanner, J. D. Bruton, A. Katz and H. Westerblad, Ca^{2+} and insulin-mediated glucose uptake, *Curr. Opin. Pharmacol.*, 2008, **8**, 339–345.

4 S. H. Huang and M. P. Czech, The GLUT4 glucose transporter, *Cell Metab.*, 2007, **5**, 237–252.

5 A. F. M. Johnstone, G. W. Gross, D. G. Weiss, O. H. U. Schroeder, A. Gramowski and T. J. Shafer, Microelectrode arrays: a physiologically based neurotoxicity testing platform for the 21st century, *NeuroToxicology*, 2010, **31**, 331–350.

6 A. Stett, U. Egert, E. Guenther, F. Hofmann, T. Meyer, W. Nisch and H. Haemmerle, Biological application of microelectrode arrays in drug discovery and basic research, *Anal. Bioanal. Chem.*, 2003, **377**, 486–495.

7 N. A. Kotov, J. O. Winter, I. P. Clements, E. Jan, B. P. Timko, S. Campidelli, S. Pathak, A. Mazzatenta, C. M. Lieber, M. Prato, R. V. Bellamkonda, G. A. Silva, N. W. S. Kam, F. Patolsky and L. Ballerini, Nanomaterials for neural interfaces, *Adv. Mater.*, 2009, **21**, 3970–4004.

8 C. E. Schmidt, V. R. Shastri, J. P. Vacanti and R. Langer, Stimulation of neurite outgrowth using an electrically conducting polymer, *Proc. Natl. Acad. Sci. U. S. A.*, 1997, **94**, 8948–8953.

9 C. D. James, R. Davis, M. Meyer, A. Turner, S. Turner, G. Withers, L. Kam, G. Banker, H. Craighead, M. Isaacson, J. Turner and W. Shain, Aligned microcontact printing of micrometer-scale poly-L-lysine structures for controlled growth of cultured neurons on planar microelectrode arrays, *IEEE Trans. Biomed. Eng.*, 2000, **47**, 17–21.

10 W. Cheng, N. Klauke, G. Smith and J. M. Cooper, Microfluidic cell arrays for metabolic monitoring of stimulated cardiomyocytes, *Electrophoresis*, 2010, **31**, 1405–1413.

11 F. Patolsky, B. P. Timko, G. H. Yu, Y. Fang, A. B. Greytak, G. F. Zheng and C. M. Lieber, Detection, stimulation, and inhibition of neuronal signals with high-density nanowire transistor arrays, *Science*, 2006, **313**, 1100–1104.

12 P. Molnar, W. S. Wang, A. Natarajan, J. W. Rumsey and J. J. Hickman, Photolithographic patterning of C_2C_{12} myotubes using vitronectin as growth substrate in serum-free medium, *Biotechnol. Prog.*, 2007, **23**, 265–268.

13 S. T. Cooper, A. L. Maxwell, E. Kizana, M. Ghoddusi, E. C. Hardeman, I. E. Alexander, D. G. Allen and K. N. North, C_2C_{12} co-culture on a fibroblast substratum enables sustained survival of contractile, highly differentiated myotubes with peripheral nuclei and adult fast myosin expression, *Cell Motil. Cytoskeleton*, 2004, **58**, 200–211.

14 T. Cohen-Karni, B. P. Timko, L. E. Weiss and C. M. Lieber, Flexible electrical recording from cells using nanowire transistor arrays, *Proc. Natl. Acad. Sci. U. S. A.*, 2009, **106**, 7309–7313.

15 Y. Haraguchi, T. Shimizu, M. Yamato, A. Kikuchi and T. Okano, Electrical coupling of cardiomyocyte sheets occurs rapidly *via* functional gap junction formation, *Biomaterials*, 2006, **27**, 4765–4774.

16 H. Fujita, K. Shimizu and E. Nagamori, Application of a cell sheet-polymer film complex with temperature sensitivity for increased mechanical strength and cell alignment capability, *Biotechnol. Bioeng.*, 2009, **103**, 370–377.

17 K. Nagamine, T. Kawashima, T. Ishibashi, H. Kaji, M. Kanzaki and M. Nishizawa, Micropatterning contractile C_2C_{12} myotubes embedded in a fibrin gel, *Biotechnol. Bioeng.*, 2010, **105**, 1161–1167.

18 M. Nishizawa, H. Nozaki, H. Kaji, T. Kitazume, N. Kobayashi, T. Ishibashi and T. Abe, Electrodeposition of anchored polypyrrole film on microelectrodes and stimulation of cultured cardiac myocytes, *Biomaterials*, 2007, **28**, 1480–1485.

19 T. Nedachi and M. Kanzaki, Regulation of glucose transporters by insulin and extracellular glucose in C_2C_{12} myotubes, *Am. J. Physiol.: Endocrinol. Metab.*, 2006, **291**, E817–E828.

20 T. Nedachi, H. Fujita and M. Kanzaki, Contractile C_2C_{12} myotube model for studying exercise-inducible responses in skeletal muscle, *Am. J. Physiol.: Endocrinol. Metab.*, 2008, **295**, E1191–E1204.

21 S. Mitsushima, S. Kawahara, K. I. Ota and N. Kamiya, Consumption rate of Pt under potential cycling, *J. Electrochem. Soc.*, 2007, **154**, B153–B158.

22 T. S. Hansen, K. West, O. Hassager and N. B. Larsen, Direct fast patterning of conductive polymers using agarose stamping, *Adv. Mater.*, 2007, **19**, 3261–3265.

ACS Macro Letters

Letter

pubs.acs.org/macroletters

Conducting Polymer Microelectrodes Anchored to Hydrogel Films

Yuichiro Ido,[†] Daisuke Takahashi,[†] Masato Sasaki,[†] Kuniaki Nagamine,[†,‡] Takeo Miyake,[†,‡] Piotr Jasinski,[§] and Matsuhiko Nishizawa*[,†,‡]

[†]Department of Bioengineering and Robotics, Graduate School of Engineering, Tohoku University, 6-6-01 Aramaki, Aoba-ku, Sendai 980-8579, Japan

[‡]JST-CREST, Sanbancho, Chiyoda-ku, Tokyo 102-0075, Japan

[§]Faculty of Electronics, Telecommunication and Informatics, Gdansk University of Technology, ul. Narutowicza 11/12, 80-233 Gdansk, Poland

Supporting Information

ABSTRACT: We report the fabrication of totally organic hydrogel-based microelectrodes of poly(3,4-ethylenedioxythiophene) (PEDOT), which exhibit a lowered sheet resistivity of about 100 Ω/□. The preparation process starts with the electrodeposition of conductive PEDOT (ca. 20 S cm^{-1}) on Pt microelectrodes. After laminating hydrogels onto the PEDOT-modified Pt electrode substrates, a second PEDOT (low conductivity) layer was electrodeposited to anchor the first PEDOT film to the hydrogel. Finally, the hydrogel sheet with PEDOT micropatterns was peeled off by taking advantage of the electroactuation property of PEDOT. The process proved to be versatile, allowing the use of most natural and synthetic hydrogels including agarose, collagen, polyacrylamide, and so on.

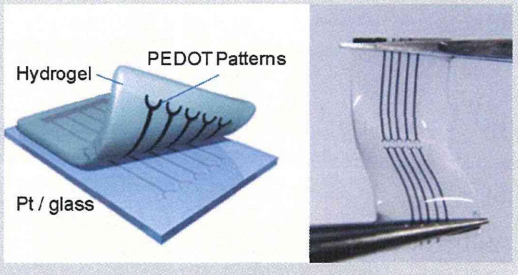

Conducting polymers (CPs) such as poly(3,4-ethylenedioxythiophene) (PEDOT) are attractive electrode-coating materials, having the advantages of biocompatibility and low electrical impedance.[1−3] They have been utilized for implanted electronics[4−6] and in vitro devices for culturing cells.[7−11] In contrast to these conventional metal-supported CP electrodes, we have attempted to prepare an autonomous CP microelectrode on a hydrogel substrate that contains ~80% H_2O in order to develop a totally organic, flexible, and molecularly permeable electrode. All of the existing printing methods using screens, inkjet systems, or microstamps, require the drying of fluid inks and, thus, cannot be used for printing on a moist gel substrate. Recently, we found that the electrodeposition of PEDOT into an agarose film produces such a gel-based electrode, which is soft enough to contract synchronously with the motion of muscle cells.[12] However, the sheet resistivity of that PEDOT electrodes formed in the agarose (ca. 10 kΩ/□) was unfortunately higher than expected.[13] Apparently, dendritic growth through the hydrogel matrix[5] resulted in a larger surface area (manifested by a larger double layer capacitance) but a lower electrical conductivity due to the sparse structure. An improvement in the conductive property of the PEDOT/hydrogel electrodes should expand their possible applications.

We report herein an improved process to prepare more conductive PEDOT micropatterns on hydrogels. As shown in Figure 1a, the dense PEDOT film was first electropolymerized on Pt microelectrodes. Owing to the absence of hydrogel, we can freely employ appropriate polymerization conditions. For example, the use of CH_3CN as solvent leads to highly conductive PEDOT, as described later; the polymerization from aqueous EDOT solutions would have advantages for the biofunctionalization of PEDOT such as enzyme immobilization.[3,14] Next, as illustrated in Figure 1b,c, after forming agarose or laminating a precured other hydrogel onto the PEDOT-modified electrode substrates, a second PEDOT layer was electropolymerized from aqueous EDOT solution to anchor the first conductive PEDOT film to the hydrogel matrix. The process we previously reported[12] depended only on this sparse PEDOT for electrode preparation. Finally, the hydrogel film with PEDOT micropatterns was peeled from the Pt electrode substrate (Figure 1d) by taking advantage of the electrochemical elastic actuation of PEDOT (±0.5 V vs Ag/AgCl).[15,16]

Figure 2 shows photographs of typical specimens after the peeling process with different polymerization charges of the second PEDOT, proving its importance for nondisruptive peeling. The 1 × 1 cm Pt electrodes on glass substrates were first coated with a 300 mC PEDOT film. Next, a melted 2.8 wt % agarose solution was poured over the substrate and gelated by cooling in room temperature (2 mm thickness). Then a second PEDOT layer was electropolymerized at charges of (a) 0, (b) 100, and (c) 200 mC. Finally, twin cycles of electrochemical elastic actuation was applied for inducing stress at the polymer/electrode interface, leading to eventually

Received: December 22, 2011
Accepted: February 24, 2012
Published: February 28, 2012

   dx.doi.org/10.1021/mz2002406 | ACS Macro Lett. 2012, 1, 400−403

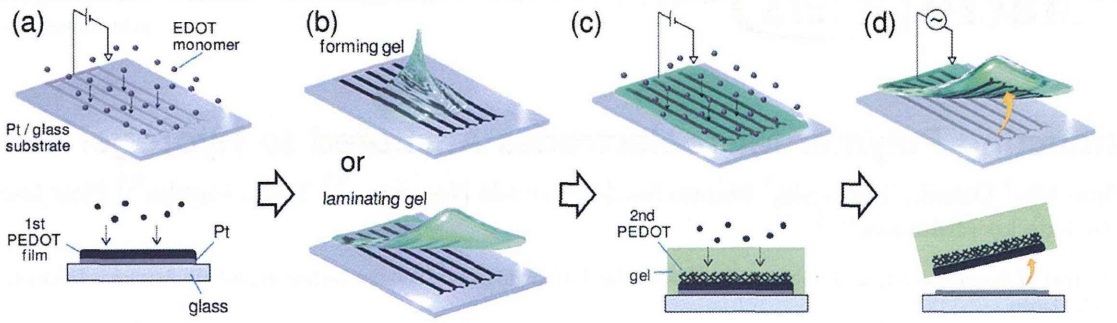

Figure 1. Schematic illustrations of the fabrication process for a conducting polymer/hydrogel electrode: (a) PEDOT was electropolymerized on a Pt microelectrode substrate; (b) a hydrogel sheet was formed or laminated on the substrate; (c) PEDOT was again polymerized; (d) then a PEDOT/hydrogel electrode was peeled from the substrate after electrochemical elastic actuation.

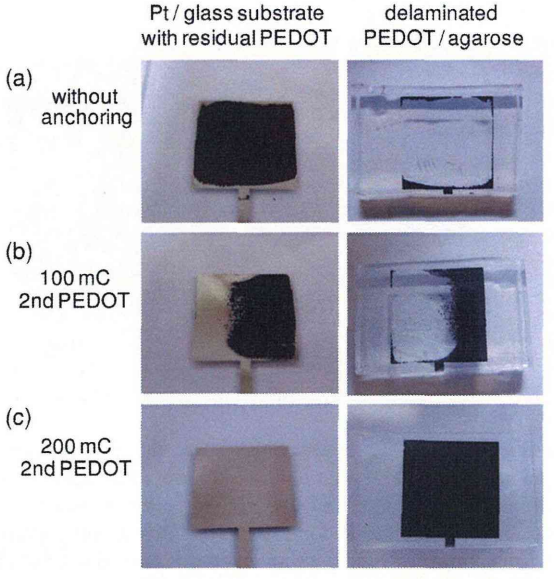

Figure 2. Photographs of Pt/glass substrates and agarose sheets after the peeling process with twin redox cycles (±0.5 V vs Ag/AgCl). The polymerization charge of the first PEDOT films was 300 mC and (a) 0, (b) 100, and (c) 200 mC for the second PEDOT layers. The polymerization was potentiostatic at 1.0 V vs Ag/AgCl in 0.1 M $LiClO_4$ aqueous solution of EDOT.

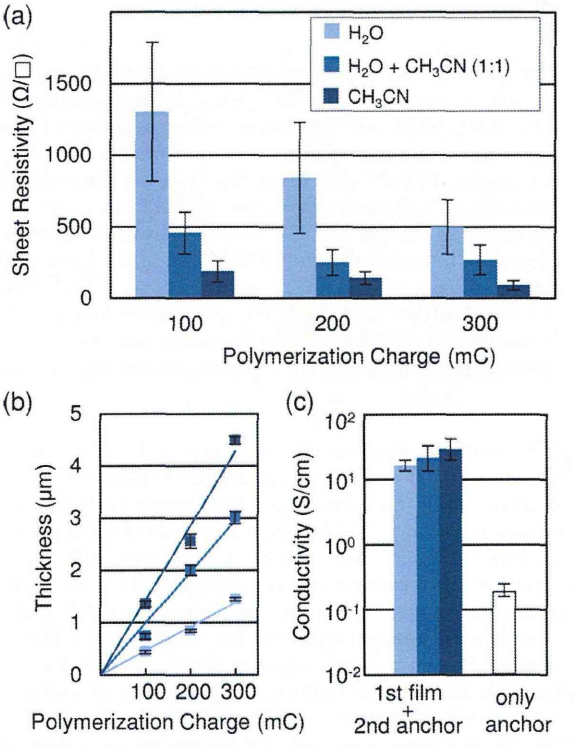

Figure 3. (a) Sheet resistivity of the PEDOT patterns (1 × 1 cm) transferred to agarose films as functions of polymerization charge of the first PEDOT film (100, 200, and 300 mC) and the solvents used for the polymerization (H_2O, CH_3CN, and their 1:1 mixture). The mean values (±standard deviation) of at least three independent specimens are given. The polymerization was potentiostatic at 1.0 V in each solution containing 50 mM EDOT and 0.1 M $LiClO_4$. The charge for second PEDOT layer was 300 mC. (b) Thickness of the first PEDOT films measured by a surface texture analyzer (DEKTAC 150). (c) Conductivity of the PEDOTs calculated by using their thickness. The conductivity value in the case without the first PEDOT film (only the second PEDOT anchor) is also shown.

detachment. In the case without the second PEDOT deposition, a clean transfer of the pattern has never achieved (Figure 2a). The second PEDOT of 100 mC resulted in an irregular, partial transfer (Figure 2b). On the other hand, the second PEDOT of 200 mC ensured 100% transfer every time (Figure 2c), indicating that a sufficient amount of a second dendritic PEDOT layer (more than 200 mC) can serve as an effective anchor to connect the first PEDOT film and the hydrogel matrix. It is worth noting that a prior hydrophilic modification of the glass substrates with aminosilane is also necessary for nondisruptive peeling; we immersed Pt/glass substrates in 20 mM 3-aminopropyltriethoxysilane/heptane for 6 h for forming the self-assembling monolayer of aminosilane on the surface of the glass part of the substrates. Without these treatments, the naturally impure glass surface often causes anisotropic lateral growth of the polymer from the Pt electrode along the surface of the surrounding glass, resulting in adhesion between the CP and the glass substrate.[11]

With the polymerization charge of the second PEDOT fixed at 300 mC, we studied next the sheet resistivity of the peeled PEDOT patterns by changing the polymerization conditions of the first PEDOT films. The resistivity measurements were conducted under wet conditions by the two-point probe method around 0.4 V versus Ag/AgCl, where the PEDOT is in

dx.doi.org/10.1021/mz2002406 | ACS Macro Lett. 2012, 1, 400–403

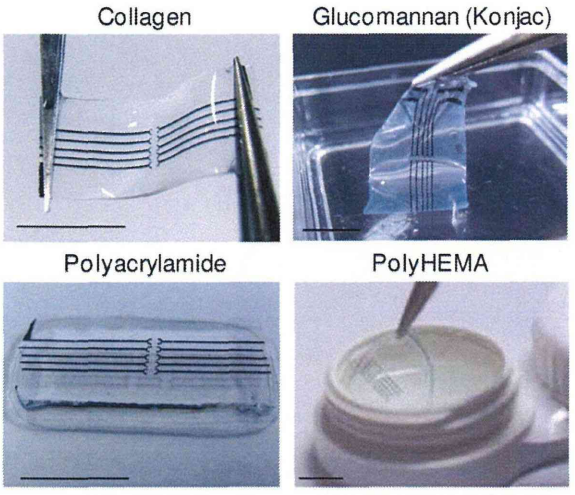

Figure 4. Photographs of the PEDOT microelectrodes anchored to the preliminarily molded hydrogel films of collagen (0.3 mm thick), glucomannan (1 mm thick), polyacrylamide (1 mm thick), and a commercial soft contact lens made of poly(2-hydroxyethyl methacrylate). Scale bar: 5 mm.

the oxidized form. The ohmic property was checked by varying the bias between the probes. Figure 3a shows that increasing the polymerization charge up to 300 mC decreased the sheet resistivity to less than 500 Ω/□, a value 2 orders of magnitude lower than that (ca. 10 kΩ/□) of the PEDOT electrode prepared by our previous process without the first PEDOT film.[12] In particular, the PEDOT film prepared using CH_3CN solvent showed the lowest resistivity, about 100 Ω/□. Presumably, polymerization at greater than 300 mC will further decrease the sheet resistivity. As shown in Figure 3b, the thickness of the first PEDOT film, measured by a surface texture analyzer, were found vary with solvents used, probably due to difference in the Coulombic efficiency of electrodeposition. The 300 mC/cm^2 polymerization led to a thickness of about 1.5 μm in H_2O, 3.0 μm in H_2O/CH_3CN, and 4.5 μm in CH_3CN, respectively. Figure 3c depicts the conductivity of the transferred PEDOTs calculated taking account of their thickness. The conductivity values of the present PEDOT electrodes reach the range of 10^1 S/cm, regardless of the kind of solvent, the value being comparable to the generally known conductivity of the PEDOT.[13] For reference, the second PEDOT layer grown in agarose showed a thickness of about 5 μm for 300 mC/cm^2,[12] as also judged from the cross section (Supporting Information, Figure S1). Because the conductivity of the second PEDOT layer grown in agarose was in the range of 10^{-1} S/cm, its contribution to the net conductivity is small; it functions simply as an anchor between the first PEDOT film and the hydrogel.

The process used to prepare PEDOT micropatterns was versatile, being also successful with precured films of other kinds of natural hydrogels (collagen, glucomannan) and synthetic hydrogels (polyacrylamide, poly(2-hydroxyethyl methacrylate)), as shown in Figure 4. In addition, the PEDOT patterning process is adaptive to the variations of elasticity, thickness and shapes of the hydrogels. For example, even a commercial soft contact lens can be used as the substrate for PEDOT electrodes. Although the structural and electrical characters of the second PEDOT would be somewhat different by the hydrogels used, they functioned well as the anchor for nondisruptive peeling of the first PEDOT, as with the case of agarose. Among the hydrogels we studied, only the fibrin gel could not be used as the substrate for PEDOT electrodes. The electrostatic and chemical conditions in fibrin may inhibit the polymerization of the second PEDOT.

The hydrogel-based CP micropatterns discussed here represent a totally organic, moist, flexible, and molecularly permeable electrode that can be combined with cells and tissues without disturbing the physiological conditions including the continuous supply of O_2 and nutrients. Such properties are ideal for use as in vivo and in vitro electrodes for stimulation and recording. Besides such cellular applications, these improved conductivity CP/gel electrodes should be applicable to a variety of hydrogel-based electronic systems such as iontophoretic drug delivery.

■ ASSOCIATED CONTENT

Supporting Information

The optical microscope image of the cross section of PEDOT/agarose electrode. This material is available free of charge via the Internet at http://pubs.acs.org.

■ AUTHOR INFORMATION

Corresponding Author

*E-mail: nishizawa@biomems.mech.tohoku.ac.jp.

Notes

The authors declare no competing financial interest.

■ ACKNOWLEDGMENTS

The authors thank BEX Co. for the kind donation of collagen sheets. This work was partly supported by The Research Grant Program of Asahi Glass Foundation and by Grants-in-Aid for Scientific Research B (No. 17310080) from the Ministry of Education, Science, and Culture, Japan.

■ REFERENCES

(1) Skotheim, T., Reynolds, J. R., Eds. *Handbook of Conducting Polymers*; Marcel Dekker: New York, 2006.
(2) Leger, J., Berggren, M.; Carter, S., Eds. *Iontronics*; CRC Press: New York, 2011.
(3) Guiseppi-Elie, A. *Biomaterials* **2010**, *31*, 2701−2716.
(4) Kim, D.-H.; Wiler, J. A.; Anderson, D. J.; Kipke, D. R.; Martin, D. C. *Acta Biomater.* **2010**, *6*, 57−62.
(5) Kim, D.-H.; Abidian, M.; Martin, D. C. *J. Biomed. Mater. Res., Part A* **2004**, *71A*, 577−585.
(6) George, P. M.; Lyckman, A. W.; LaVan, D. A.; Hegde, A.; Leung, Y.; Avasare, R.; Testa, C.; Alexander, P. M.; Langer, R.; Sur, M. *Biomaterials* **2005**, *26*, 3511−3519.
(7) Schmidt, C; Shastri, V. R.; Vacanti, J. P.; Langer, R. *Proc. Natl. Acad. Sci. U.S.A.* **1997**, *94*, 8948−8953.
(8) Kim, S. Y.; Kim, K.-M.; Hoffman-Kim, D.; Song, H.-K.; Palmore, G. T. R. *ACS Appl. Mater. Interface* **2010**, *3*, 16−21.
(9) Svennersten, K.; Bolin, M. H.; Jager, E. W. H.; Berggren, M.; Richter-Dahlfors, A. *Biomaterials* **2009**, *30*, 6257−6264.
(10) Nyberg, T.; Shimada, A.; Torimitsu, K. *J. Neurosci. Methods* **2007**, *160*, 16−25.
(11) Nishizawa, M.; Nozaki, H.; Kaji, H.; Kitazume, T.; Kobayashi, N.; Ishibashi, T.; Abe, T. *Biomaterials* **2007**, *28*, 1480−1485.
(12) Sekine, S.; Ido, Y.; Miyake, T.; Nagamine, K.; Nishizawa, M. *J. Am. Chem. Soc.* **2010**, *132*, 13174−13175.
(13) Groenendaal, L. B.; Jonas, F.; Freitag, D.; Pielartzik, H.; Reynolds, J. R. *Adv. Mater.* **2000**, *12*, 481−494.
(14) Gerard, M.; Chaubey, A.; Malhotra, B. D. *Biosens. Bioelectron.* **2002**, *17*, 345−359.

(15) Jager, E. W. H.; Smela, E.; Inganas, O. *Science* **2000**, *290*, 1540–1545.
(16) Han, G.; Shi, G. *Sens. Actuators, B* **2006**, *113*, 259–264.

Electrochimica Acta 82 (2012) 175–178

Contents lists available at SciVerse ScienceDirect

Electrochimica Acta

journal homepage: www.elsevier.com/locate/electacta

Sheet-shaped biofuel cell constructed from enzyme-modified nanoengineered carbon fabric

Keigo Haneda[a], Syuhei Yoshino[a], Takuya Ofuji[a], Takeo Miyake[a,b,*], Matsuhiko Nishizawa[a,b,*]

[a] Department of Bioengineering and Robotics, Tohoku University, 6-6-1 Aramaki Aoba, Aoba-ku, Sendai 980-8579, Japan
[b] Core Research for Evolutional Science and Technology (CREST), Japan Science and Technology Agency, Tokyo 102-0075, Japan

ARTICLE INFO

Article history:
Received 27 November 2011
Received in revised form 7 January 2012
Accepted 9 January 2012
Available online 14 February 2012

Keywords:
Biofuel cell
Carbon fabric
Carbon nanotube
Gas-diffusion cathode

ABSTRACT

A strip of carbon fabric (CF) electrode modified with multiwalled carbon nanotubes and subsequently fructose dehydrogenase (FDH) showed an oxidation current density of ~11 mA cm^{-2} in stirred 200 mM fructose solution. Obtaining a sufficient dispersion of the nanotubes during its modification was found to be critical to ensure such a performance of the FDH anode. For use with this anode, a CF strip modified with ketjenblack (KB) and bilirubin oxidase (BOD) served as a gas-diffusion cathode for the reduction of O_2 from air at a current density of ~2 mA cm^{-2}. The FDH-modified CF strip and the BOD-modified CF strip were stacked with an agarose film that retained an electrolyte solution and fuel (fructose) to construct a totally flexible sheet-shaped biofuel cell. This assembly allowed bending of 44° without affecting the maximum output power density, 550 μW cm^{-2} obtained at 0.4 V.

1. Introduction

Enzyme-based biofuel cells that generate electricity through enzymatic oxidation of biological fuels like sugars and alcohols have attracted attention as ubiquitous, safe power sources [1–23]. Recent rapid improvements in their power performance up to mW cm^{-2} levels by employing nanostructured carbon electrodes [24–28] have motivated various applications including a sheet-shaped cell that can be combined with advanced flexible film electronics [29,30]. However, the brittle carbon electrodes, which are generally aggregates of particulate or tubular nanocarbons, often limit the design and uses of such biofuel cells.

In the present work, we have prepared a totally flexible, sheet-shaped biofuel cell by using a carbon fabric (CF) as the flexible, conductive base for the enzyme electrodes. We modified the CF strip with multiwalled carbon nanotubes (CNTs) and fructose dehydrogenase (FDH) for the oxidation of fructose, and with ketjenblack (KB) and bilirubin oxidase (BOD) for the reduction of oxygen in the ambient air. Both FDH and BOD are capable of efficient "direct electron transfer" with common electrode materials including carbon [10,16,21,31,32]. The pre-modifications with CNT or KB increase the specific surface area of the CF electrodes, resulting in effective enzyme immobilization and, ultimately, higher power. The FDH anode strip and the BOD cathode strip are stacked with a hydrogel film that retains the electrolyte solution and fuel (fructose), as shown in Fig. 1. This assembly provides a stand-alone, sheet-shaped power source that can be bent without loss of output power.

2. Experimental

2.1. Preparation of carbon fabric anode

A 5 mm × 5 mm strip of carbon fabric (CF) (TCC-3250, donated from Toho Tenax Co.) was first modified with multiwalled carbon nanotubes (Baytubes, donated from Bayer Material Science Co.) to increase the specific surface area. The carbon nanotubes (CNTs) were pretreated by heating at 400 °C for 11 h and by immersing in mixed acid ($H_2SO_4 + HNO_3$ in a 1:3 ratio) for 5 h. The treated CNT were dispersed in water containing Triton X-100 surfactant (0.05, 0.1, 0.5 or 1%). A 40 μl aliquot of the 10 mg ml^{-1} CNT dispersion was dropped on a CF strip (0.32 mm thickness, 0.25 cm^2 geometric area) and dried in air, followed by thoroughly washing out the surfactant by soaking in a pure McIlvaine buffer solution for more than 1 h with stirring. Then, the CNT-modified CF strip was immersed in a 5 mg ml^{-1} solution of D-fructose dehydrogenase (FDH) (EC1.1.99.11, 169.9 U mg^{-1}, ca. 140 kDa, from Gluconobacter, purchased from Toyobo Enzyme Co.) for FDH immobilization [28]. It has been reported that FDH works as a electrocatalyst for oxidation of fructose without electron transfer mediators [10,16,21,31]. The flavin-containing subunit of FDH accepts electrons from fructose, and transfers these electrons to the heme C-containing subunit that can electrically communicate with electrode [31].

* Corresponding authors at: Department of Bioengineering and Robotics, Tohoku University, 6-6-1 Aramaki Aoba, Aoba-ku, Sendai 980-8579, Japan.
Tel.: +81 22 795 7003; fax: +81 22 795 7003.
E-mail address: nishizawa@biomems.mech.tohoku.ac.jp (M. Nishizawa).

0013-4686/$ – see front matter © 2012 Published by Elsevier Ltd.
doi:10.1016/j.electacta.2012.01.112

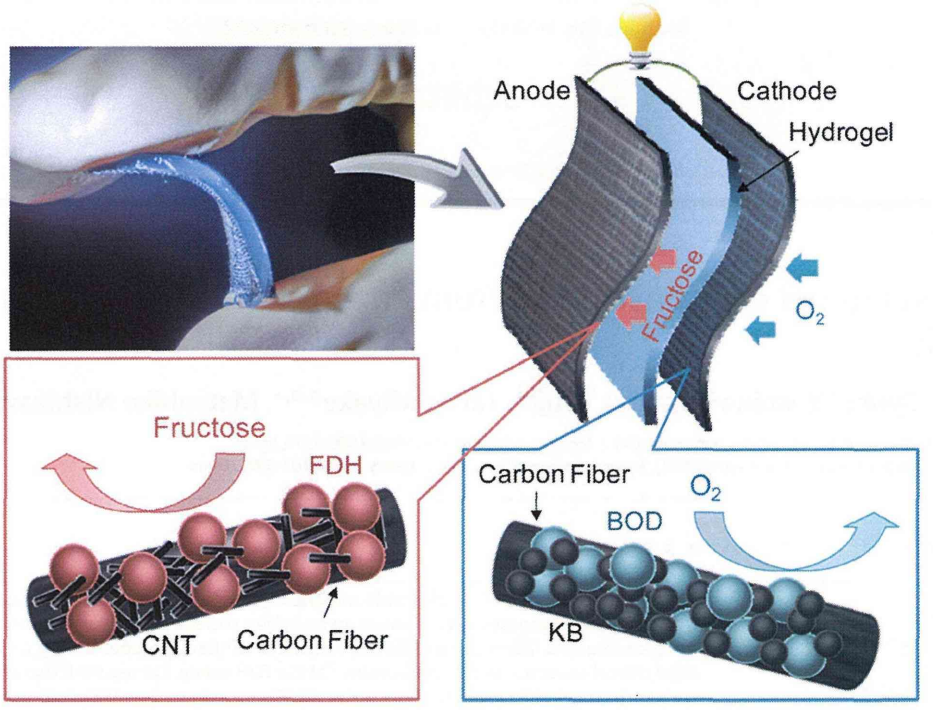

Fig. 1. A sheet-shaped biofuel cell constructed by stacking enzyme-modified nanoengineered carbon fabric strips with a hydrogel film that retains electrolyte solutions and fructose fuel.

2.2. Preparation of gas-diffusion carbon fabric cathode

The preparation of the cathode basically followed the procedures used for our previous carbon paper-based BOD cathode [23]. BOD is one of multi-cupper oxidases that can directly catalyze four-electron reduction of O_2 to H_2O even without electron transfer mediators [10,16,32]. A 25 μl aliquot of a 8 mg ml^{-1} solution of ketjenblack (KB)/poly(tetrafluoroethylene) (PTFE) (1: 1) was put on a CF strip and dried in air. The surface of the KB-modified CF electrode was further modified with a 0.1 ml solution of 5 mg ml^{-1} bilirubin oxidase (BOD, EC 1.3.3.5, 2.5 U/mg, from *Myrothecium*). After drying in air, the strip was additionally coated with the KB solution to make surface hydrophobic. The geometric size was the same as the anode (0.32 mm thickness, 0.25 cm^2 area).

2.3. Electrochemical measurements

The performance of the CF electrodes was analyzed by a three-electrode system (BSA, 730C electrochemical analyzer) in solution using a Ag/AgCl reference and a platinum counter electrode. The FDH-modified anodes were evaluated in stirred McIlvaine buffer (pH 5.0) containing 200 mM fructose, while the BOD-modified cathodes were in air-saturated McIlvaine buffer (pH 5.0). The performance of a biofuel cell constructed with the FDH-modified CF anode, the BOD-modified CF cathode, and the fructose-containing agarose film (3 mm thick) was evaluated from the cell voltage upon connecting with a variable external resistance between 180 Ω and 10 kΩ. For preparing the fructose-containing agarose films, a 150 mM McIlvaine buffer containing 200 mM fructose was first warmed to dissolve 1.5 wt% agarose, and molded with cooling. The current and the power were derived from the detected cell voltage and the resistance. Unless otherwise indicated, the electrochemical measurements were carried out at room temperature, around 25 °C.

3. Results and discussion

3.1. Performance of FDH/CNT/CF bioanodes

Fig. 2 shows cyclic voltammograms of the FDH/CNT/CF electrodes (solid plots) at 10 mV s^{-1} in a stirred buffer solution containing 200 mM fructose. In comparison with the FDH/CF electrode prepared without CNTs (broken line plot), the increased specific surface area produced by CNT-modification obviously increased the current density by at least an order of magnitude. In fact, the measured double-layer capacitance of the CNT-modified electrodes has a 2 orders larger value (ca. 6.5 mF cm^{-2}) than that of the original CF (0.07 mF cm^{-2}). Importantly, the oxidation current

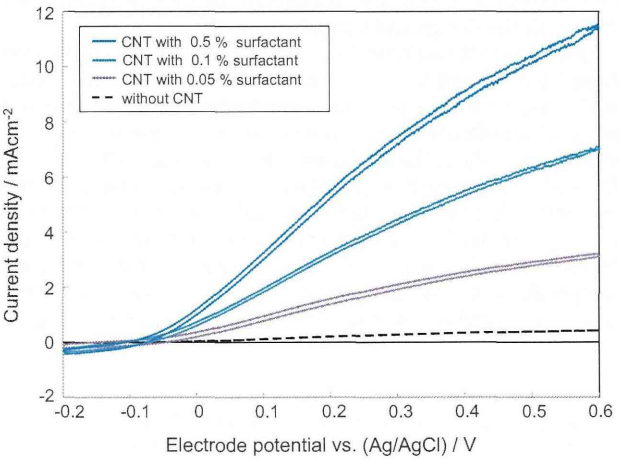

Fig. 2. Cyclic voltammograms of FDH-immobilized CF strip electrodes at 10 mV s^{-1} in a stirred buffer solution (pH 5) containing 200 mM fructose. The CF electrodes were pre-modified with CNTs dispersed with different concentrations of Triton X-100 surfactant.

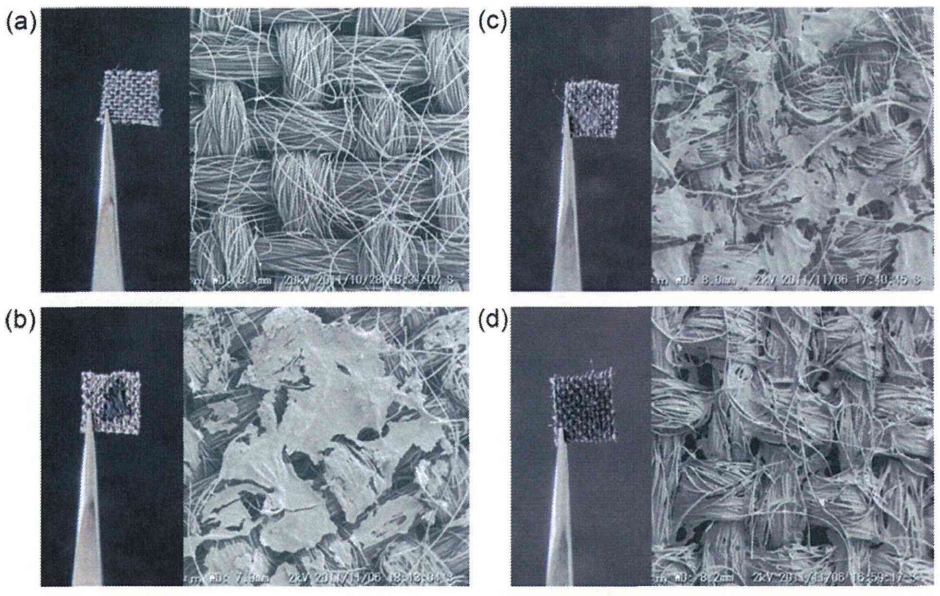

Fig. 3. Photographs and SEM images of (a) a bare CF strip and (b–d) CNT-modified strips. The CNT dispersions were prepared with (b) 0.05%, (c) 0.1%, (d) 0.5% Triton X-100 surfactant.

density depended on the concentration of the Triton X-100 surfactant used for the CNT dispersion (0.05, 0.1 and 0.5%), despite the fact that all these CNT-modified electrodes had similar capacitance (similar specific surface area). The use of 1% surfactant brought no significant further change over that from 0.5% surfactant. Fig. 3 shows the surface structure of the CNT-adsorbed CF strips observed by optical and scanning electron microscopies. The CNT dispersions with 0.05% and 0.1% surfactant are found to precipitate on the CF surface (Fig. 3b and c). In contrast, the CNT dispersion with 0.5% surfactant seems to entirely penetrate into the CF strip. This uniform modification with CNT would be a main reason of the enhanced anode performance, up to a value of 11.5 mA cm^{-2} at 0.6 V.

3.2. Performance of gas-diffusion biocathodes

Fig. 4 shows cyclic voltammograms of a BOD-modified CF cathode at 10 mV s^{-1}. The electrode strip was put on an oxygenic pH 5.0 buffer solution so as to contact the solution by the BOD-modified face (purple solid plot). The reduction current density reaches ~0.76 mA cm^{-2} (at 0 V), which is 1.5 times larger than that measured by the biocathode immersed into the solution (broken line plot). This increase of current density is a result of a better oxygen supply from the ambient air through the CF. Moreover, an additional KB coating onto the BOD-modified face of the CF strip enhanced the performance further to 2.0 mA cm^{-2}, which was reproducible within 10% variation (1.8–2.2 mA cm^{-2}) for four independent electrode specimens. Presumably, the hydrophobic nature of that coating controls excess penetration of solution into the CF electrodes [23]. The reduction current density at 0 V varied 1.8–2.2 mA cm^{-2}.

3.3. Performance of the flexible biofuel cell

A biofuel cell was constructed with the FDH/CNT-modified CF anode and the KB/BOD/KB-modified gas-diffusion CF cathode. These electrodes were attached to both sides of an agarose hydrogel (3 mm thick) made with 150 mM McIlvaine buffer solution (pH 5.0) containing 200 mM fructose. The enzyme-modified hydrophilic anode appeared to become moistened by blotting of the solution from the hydrogel layer. On the other hand, the O_2 reduction at the hydrophobic cathode proceeded at the three-phase boundary of the hydrogel–electrode interface. Fig. 5 shows typical examples of the cell performance. The open-circuit voltage of the cell was 0.7 V, which is similar to the difference between the potentials at which fructose oxidation and oxygen reduction start to occur in cyclic voltammograms (−0.1 V in Fig. 2 and 0.6 V in Fig. 4, respectively). The maximum values of current and power densities are determined by the BOD-cathode because of its comparatively lower performance than FDH-anode. Even as a stand-alone assembly with the fuel (fructose)-containing gel sheet, the maximum power density reached 550 μW cm^{-2} at 0.4 V. Importantly, this device could be repeatedly bent to a 44° angle without significant loss of output power. Bending in excess of this value caused fracture of the agarose hydrogel sheet; our device can be made more resistant to mechanical stress by using more elastic hydrogels such as polyvinylalcohol.

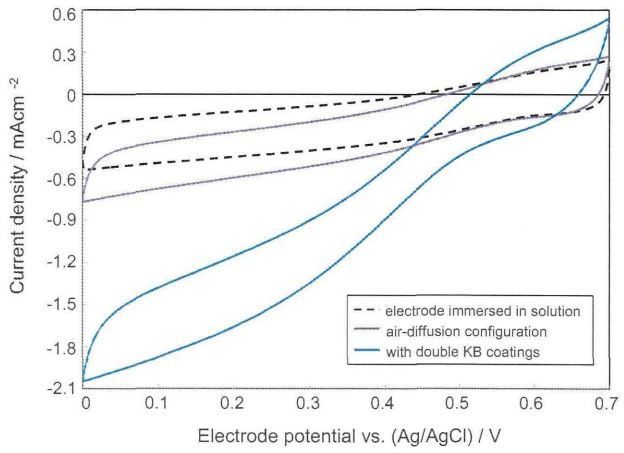

Fig. 4. Cyclic voltammograms of O_2 reduction at a BOD/KB-modified CF strip measured at 10 mV s^{-1} in the solution (broken line) and on the solution (air-diffusion configuration, solid lines). The activity of the CF electrode was enhanced by further modification with KB after the BOD immobilization.